Growth, structure, and morphology of the Pd/MgO(001) interface: Epitaxial site and interfacial distance

G. Renaud,* A. Barbier, and O. Robach
CEA-Grenoble, Département de Recherche Fondamentale sur la Matière Condensée/SP2M/IRS,†
17, rue des Martyrs, 38054 Grenoble Cedex 9, France
(Received 30 September 1998; revised manuscript received 26 February 1999)

The growth at room temperature of Pd on an atomically flat MgO(001) surface has been investigated by grazing incidence x-ray scattering. The structure and morphology of deposits in the range 0.2 to 183 monolayers (ML) were analyzed *in situ*, in ultrahigh vacuum (UHV). The growth proceeds by nucleation, growth, and coalescence of islands. Channeling between islands starts around 18 ML, and above 35 ML, the film is continuous and fully covers the substrate. Pd is in cube-on-cube epitaxy on MgO(001), with an average lattice parameter between those of bulk Pd and MgO. Neither stacking faults nor twins were found. As growth proceeds, Pd is increasingly relaxed, but most of the Pd in the first one or two atomic planes is fully lattice matched with the substrate. The islands are coherent with the substrate up to ~4–5 ML of Pd deposited. Above 5 ML, interfacial misfit dislocations are introduced at their edges. These dislocations reorder to form a square network above 35 ML. We have determined the epitaxial site, above oxygen ions of the substrate, and the interfacial distance (2.22 ± 0.03 Å). The evolution of the interfacial distance as a function of the amount of Pd deposited is deduced by a quantitative analysis of the substrate crystal truncation rods. Similarities and differences with the Ag/MgO and Ni/MgO interfaces are discussed, and general trends on the interfacial structure and morphology are deduced. [S0163-1829(99)14431-X]

I. INTRODUCTION

Ceramics and metal/ceramics interfaces are present in many industrial materials such as catalytic converters, field effect transistors, low-emittance glasses, anticorrosion coatings, composite materials, or medical implants. The properties of these materials are often intimately related to the structure, composition, and morphology of their internal interfaces.[1] However, these properties are difficult to predict because the interfacial energy contains several terms[2–7] that are of the same order of magnitude. Like the Ag and Ni/MgO interfaces we have studied earlier, the Pd/MgO interface has been chosen as a model metal-oxide system because it is relatively simple:[8,9] it has fourfold symmetry, a small unit cell, and no chemical reaction takes place at the interface. Moreover, the epitaxy is cube on cube over a very wide temperature range (100 to 700 K),[10] and the MgO(001) surface can be considered as a simple truncation of the bulk.[11]

In order to test the theoretical models, there is a strong need for experimental data, in particular on the adsorption site and interfacial distance. Some recent theoretical results concluded that Pd adsorbs on top-surface oxygen,[8,9,12,13] while others[14,15] concluded to adsorption above Mg ions. A SEELFS investigation[16] concluded to adsorption above the Mg site. However, experimental data are scarce because the insulating character of the substrate hampers most experimental methods. To our knowledge, although most calculations estimate the interfacial distance, no experimental determination of this parameter is available.

The Pd/MgO(001) interface is also considered as a model system to study the elementary processes in heterogeneous catalysis,[17] which depend on the exact shape and distribution of the metal clusters that are spread over a ceramic substrate. It is thus important to investigate the structure and morphology of the Pd/MgO(001) interface during growth. This has driven a large number of studies[18–26] aiming at producing small particles with a well-defined distribution of sizes.

In most theoretical investigations, the contribution of epitaxial strains to the interfacial energy is neglected, despite the relatively large lattice parameter mismatch, $(a_{\mathrm{Pd}} - a_{\mathrm{MgO}})/a_{\mathrm{MgO}} = -7.64\%$, between fcc Pd and rocksalt MgO. However, the relaxation of the lattice parameter mismatch is believed to yield an important contribution to the interfacial energy.[27] The state of strain in the metal deposit critically depends on the magnitude of the misfit as well as on the strength of the metal-oxide bonding at the interface. This may also strongly influence the growth morphology. It is thus interesting to compare the structure and morphology of similar systems such as Ag/MgO, Pd/MgO, and Ni/MgO, with very different misfit and strength of the interfacial bond. As concerns the Pd/MgO interface, the interatomic spacing in the Pd particles has been studied as a function of particle size and distance from the interface by high-resolution transmission electron microscopy (HRTEM) and surface extended energy loss fine structure (SEELFS).[18–20,28]

Grazing incidence x-ray scattering[29] (GIXS) is well suited for characterizing the structure and morphology of metal/oxide interfaces during their growth by molecular-beam epitaxy because it is insensitive to the insulating character of the substrate and can be used *in situ*, in ultrahigh-vacuum (UHV), without perturbing the deposit. We have recently shown in the case of the Ag/MgO(001) (Ref. 30) and Ni/MgO(001) (Ref. 31) interfaces that this technique allows studying the very first stages of deposition, and, more importantly, determining the epitaxial site as well as the interfacial distance and its evolution with the metal thickness. The ini-

tial growth of Pd on MgO(001) has already been investigated *ex situ* by GIXS using a laboratory source.[32,33] However, we will show that the present investigation yields a lot more information.

This paper presents GIXS results obtained *in situ*, during the growth of Pd on MgO(001) from the very early stages. The experimental conditions are first described. The results concerning the morphology of the deposit and the accommodation of the lattice parameter mismatch at the Pd/MgO interface are next presented. Then, the epitaxial site and interfacial distance are deduced, together with the evolution of several other parameters with the deposited amount. These results are discussed in a last part and are compared with the results obtained earlier on the Ag and Ni/MgO(001) interfaces. The differences between these three systems are discussed according to the magnitude of the lattice parameter misfit and the strength of the interfacial bonding.

II. EXPERIMENT

GIXS experiments were performed using the w21v surface diffraction setup[34] of the D32 undulator beamline at ESRF (European Synchrotron Radiation Facility, Grenoble, France).[35] The UHV chamber (base pressure 10^{-10} mbar), equipped with entrance and exit 0.5 mm-thick beryllium windows, is mounted on a six-circle diffractometer of ''2 +2'' type,[34,36] which allows simultaneously performing the deposits and the diffraction measurements. Pd was evaporated from an electron-beam-heated rod (99.99% purity) by a commercial evaporator (Omicron Instruments EFM4, Germany). The substrate was held at room temperature during the deposits. The measurements were performed on cumulative Pd deposits, the growth being interrupted during x-ray scans. The Pd deposition rate was 1Å/min, calibrated with a quartz microbalance prior and after the x-ray measurements. This calibration was checked by *in situ* x-ray reflectivity measurements on the last deposit. A thickness of 356 ± 1 Å was deduced, which corresponds to within 1% to the calibrated thickness. This confirms that the condensation coefficient of Pd on MgO(001) is almost 1 at room temperature.[37]

The $15 \times 15 \times 0.5$-mm^3 MgO(001) single crystal was supplied, oriented $\pm 0.1°$ and both sides polished by Sumitomo. The preparation of the MgO(001) surface has been described in detail elsewhere.[11] It leads to MgO(001) surfaces that are very flat, stoichiometric, of high-crystalline quality, and free from impurities. The widths of in-plane MgO Bragg peak were resolution limited, with a rocking curve smaller than 0.0015°. The substrate flatness was better than 0.01° over the whole sample.

The Miller indexes (h k l) are expressed in reciprocal lattice units (r.l.u) of MgO, using the bulk fcc unit cell ($a_{\mathrm{MgO}} = 4.2117$ Å). The l index is the component of the momentum transfer perpendicular to the surface. Q is the modulus of the momentum transfer.

The x-ray beam energy was set at 18 keV, which allowed measurements of crystal truncation rods[38,39](CTR's) over an extended range of perpendicular momentum transfer, thus yielding a high accuracy on out-of-plane parameters. All measurements were systematically performed with three fixed values of the incident angle α of the x-ray beam with respect to the surface, $\alpha = 0.07°$, $\alpha = 0.12° = \alpha_c^{\mathrm{MgO}}$, the critical angle for total external reflection of MgO, and $\alpha = 0.2°$. In addition, some measurements were performed at $\alpha = 0.3°$, i.e., above the critical angle for total external reflection of Pd ($\alpha_c^{\mathrm{Pd}} = 0.207°$ at this energy). Working at $\alpha = 0.07°$ was mandatory for small Pd thickness, in order to optimize the surface signal-over-noise ratio, by minimizing the background arising mainly from Compton scattering and points defects in the bulk. The sample surface was vertical. The incident x-ray beam size was 0.05-mm (H)×0.5-mm (V). The opening of the two pairs of detection slits was fixed at 1-mm (H)×1-mm (V) for the measurements of the MgO CTR's (corresponding to an angular acceptance of 0.1°), and at 6-mm (H)×1-mm (V) for in-plane measurements. The orientation matrix was so well defined that all MgO(001) diffraction peaks were at their calculated positions within 0.001°.

III. RESULTS AND ANALYSIS

A. In-plane measurements: structure and morphology

The Pd growth was investigated *in situ*, for deposits θ between 0 and 183 ML (i.e., thickness ranging from 0 to 356 Å). We first performed in-plane measurements for increasing amounts of deposited Pd, in order to analyze the epitaxial relationships and the growth morphology. Radial scans, rocking scans, as well as scans of the incident angle were systematically performed around or on the (200), (220), (400), (600), and (440) in-plane Pd diffraction peaks. Radial scans were performed at $l = 0.15$ in order to reduce the contribution from the MgO Bragg reflections. Rocking scans were exactly performed on the Pd Bragg peak (i.e., at l varying from 0.025 to 0.044, depending on the exact value of the critical angle α_c).

Figure 1 shows radial scans along the (h 0 0.15) and (h h 0.15) directions, around $h = 2$, for increasing deposited amounts, θ (in equivalent monolayers ML). Partially relaxed Pd in cube-on-cube epitaxy (i.e., with the epitaxial relationships: (001)Pd//(001)MgO and [100]Pd//[100]MgO) is present for all deposited amounts, as revealed by the peaks appearing along both directions around $h = 2.15$. The Pd peaks progressively shift toward the bulk Pd position, at $h = 2.1645$. In both radial and rocking scans, they narrow and increase in intensity as the thickness increases.

Figure 2 shows the evolution with θ of several parameters of the growing Pd. The critical angle for total external reflection α_c [Fig. 2(a)] was deduced from scans of the incident angle on the Pd in-plane Bragg peaks. The Pd peak position h [Fig. 2(b)] was deduced from radial scans. The full width at half maximum (FWHM) ω, of rocking scans on the Pd peaks [Fig. 2(c)] was deduced by fitting these peaks with a Lorentzian shape.

Below $\theta = 18$ ML, the critical angle [Fig. 2(a)] is found constant, equal to α_c^{MgO}. It next linearly increases to reach a plateau, equal to α_c^{Pd}, above 35 ML. This can be understood if we consider that the growth of Pd on MgO(001) (Refs. 18,16 and 20–24) is known to proceed via nucleation, growth and coalescence of islands, with four stages:[40] first initial nucleation of small islands, then growth and coalescence of these nuclei, then, when the islands size becomes large enough, channeling between these islands, leading to a

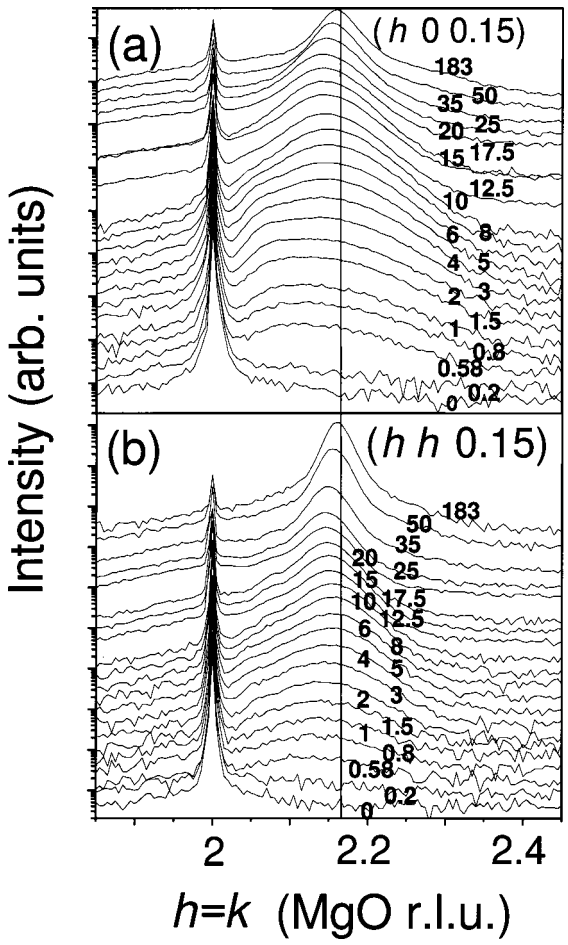

FIG. 1. Radial scans during the room-temperature growth of Pd on MgO(001), along the (h 0 0.15) (a, top) and (h h t0.15) (b, bottom) directions, as a function of the amount θ of deposited Pd. The different amounts, 0, 0.2, 0.58, 0.8, 1, 2, 3, 4, 5, 6, 8, 10, 12.5, 15, 17.5, 20, 25, 35, 50, and 183 ML, are indicated near the corresponding curves. The successive scans were vertically shifted (multiplication by a factor of 2) for clarity. A vertical line indicates the position, $h=2.1645$, expected for bulk Pd. All the scans shown here were performed with the same fixed incident angle of 0.07°.

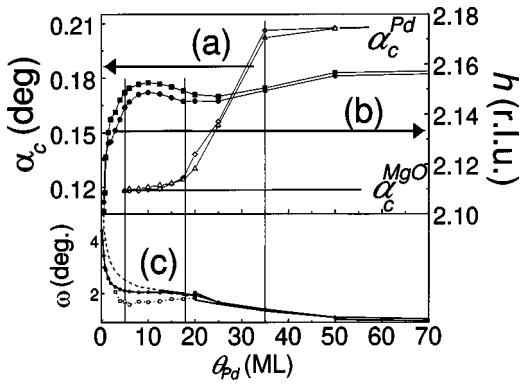

FIG. 2. Evolution with the amount θ of Pd deposited, of (a) the critical angle for total external reflection, as measured by locating the maximum of the intensity of α-scans performed on the (220) (open diamonds) and (200) (open triangles) Pd Bragg peaks (upper-curve, left scale); (b) the mean h position of the (2 2 0.15) (black squares) and (2 0 0.15) (black disks) Pd Bragg peaks in radial scans, as deduced by Lorentzian least-square fits of the peaks (upper curve, right scale); and (c) FWHM $\omega(Q)$ of the (200) (dashed line), (220) (continuous line with filled circles) and (400) (dotted line with open squares) Pd Bragg peaks measured in rocking scans (lower curve, left scale).

continuous network structure, and finally formation of a continuous, hole-free film by filling the holes. Recent TEM experiments[41,26] clearly revealed the channel stage: the islands become elongated and join to form a continuous network structure in which the deposited material is separated by long, irregular and narrow channels. As deposition continues, secondary nucleation occurs in these channels, eventually leading to a continuous film. We propose that the range between 0 and 18 ML corresponds to the two first stages. Between 18 and 35 ML, the increase of the critical angle reveals the coalescence and channeling processes: the critical angle is intermediate between those of MgO and Pd because the average density of the deposit is intermediate. In this regime, the average electron density of the deposit is smaller than that of Pd, and even than that of MgO, because significant free space is left between islands. As a result, the critical angle for total external reflection of the deposit is smaller than α_c^{MgO} and the underlying MgO externally reflects the incident beam. Between 18 and 35 ML, the increase of the critical angle reveals the coalescence processes: the critical angle is intermediate between those of MgO and Pd because the average density of the deposit is intermediate. Above 35 ML, the value of $\alpha=\alpha_c^{Pd}$ indicates that the film is continuous and almost completely covers the substrate. An intuitive interpretation (which is rigorously not correct, since only the wave representation is valid), would be that, below 18 ML, the islands are small, and do not have a significant flat portion at their top. As a result, for $\alpha<\alpha_c^{MgO}$, a large fraction of the incident beam is transmitted through the islands rather than being externally reflected by them. Between 18 and 35 ML, larger islands are present, with a significant fraction of their top surface being flat, and thus onto which the beam can be reflected, yielding a larger critical angle.

The average peak positions h of the (200) and (220) Pd Bragg peaks [Fig. 2(b)] first increase quickly from $\theta=0$ to 5 ML, then stay roughly constant (around 2.15) up to $\theta=35$ ML, before slowly increasing toward the h value (2.1645) expected for bulk Pd. For each deposited amount, the average lattice parameter of the Pd film [Fig. 3(a)] can be deduced from these peak positions. Below 5 ML, the Pd is strained by the MgO because of its larger in plane lattice parameter. Above 5 ML, on the average, Pd is much more relaxed. However, even at 183 ML, the Pd is not fully relaxed. Note that the radial scans of Fig. 1 were performed at $\alpha=0.07°$, which is much smaller than α_c^{MgO} and α_c^{Pd}. Thus, below 35 ML, before the substrate is covered, the whole film thickness is probed, while above 35 ML, only the top portion of the Pd film is probed. The scattering depth is of the order of 15 ML (30 Å) under these experimental conditions. Hence, the average lattice parameter reported in Fig. 3(a) is that of the top 30 Å of the Pd film, at least above 35 ML. Below 35 ML, even with this grazing incidence angle, because the critical angle is intermediate between that of MgO and that of Pd, the whole film thickness is probed.

Figure 4 shows the (h 0 0.15) and (h h 0.15) radial scans performed on the 183 ML thick film at $\alpha=0.07°$, 0.2°, and

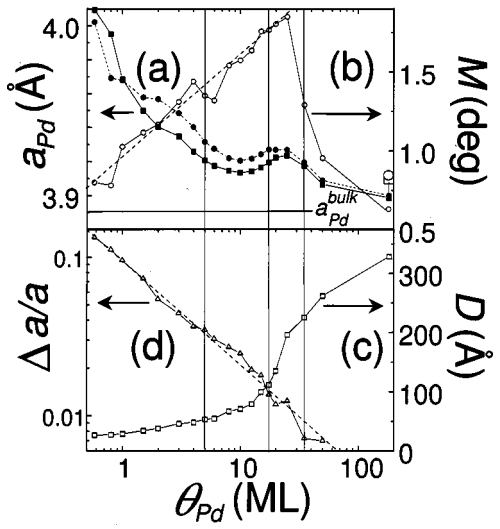

FIG. 3. Evolution of four parameters characterizing the structural quality of the top 30 Å of the Pd film, as a function of the amount θ of Pd deposited. (a) Average in-plane Pd lattice parameter a_{Pd} deduced from the (200) (upper, left scale, solid circles) and the (220) (upper, left scale, solid squares) reflections. The lattice parameters averaged over the whole film thickness from scans at $\alpha = 0.3°$ for the 183 ML film are also reported as large open symbols. A horizontal line locates the lattice parameter of bulk Pd. (b) Average mosaic-spread (upper, right scale, open circles). (c) Average in-plane domain size D (lower, right scale open squares); and (d) average gradient $\Delta a/a$ of Pd lattice parameter (lower, left scale, open triangles). A vertical line at 5 ML locates the onset of the introduction of dislocations at the edges of islands, and two other vertical lines at 18 and 35 ML locate the onset and end of island channeling.

0.3°. For $\alpha = 0.07°$ and 0.2°, which are below α_c^{Pd}, similar peak positions are found. For $\alpha = 0.3°$, for which the whole 183 ML-thick film is probed, the Pd peaks are closer to those of MgO: the Pd looks more strained. This yields the lattice parameter averaged over the whole thickness (3.9123 Å), also reported in Fig. 3(a) which corresponds to a 0.6% average lattice expansion. The parameter averaged over the top 30 Å is 3.8991 Å (only 0.2% expansion with respect to bulk Pd), more than twice closer to the Pd bulk lattice parameter of 3.89 Å. These scans with different incident angles thus show that the relaxation in Pd is gradual: the parameter decreases with increasing height with respect to the interface.

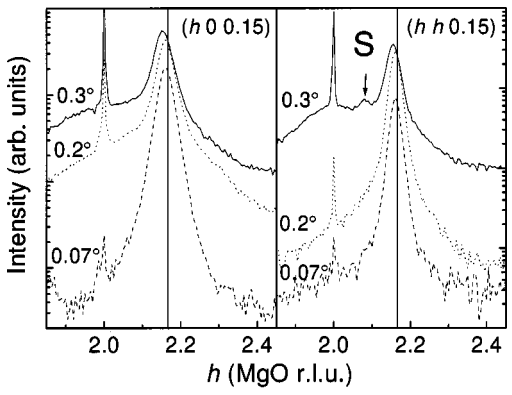

FIG. 4. Radial scans along the (h 0 0.15) (left) and (h h 0.15) (right) directions around $h = 2$, for the thickest (183 ML) film, and different incident angles $\alpha = 0.07°$ (dashed lines), $\alpha = 0.2°$ (dotted lines) and $\alpha = 0.3°$ (continuous lines). The logarithm of the intensity is reported as a function of the in-plane coordinate h. Remark the satellite, noted S, between the Pd and MgO (2 2 0.15) peaks, visible when $\alpha = 0.3°$.

The angular width $\omega(Q)$ of the Pd diffraction peaks in rocking scans [Fig. 2(c)] is large (several degrees) for small θ, and decreases continuously as the deposited thickness increases. Above 35 ML, when the film is continuous, the widths of the different orders of Pd reflections [(200), (220), and (400)] are very close to each other, while they differ below 18 ML. The rocking width may have two origins: the limited size $D = 2\pi/\Delta Q_s$ of crystallites with a contribution $\omega_s(Q) = \Delta Q_s/Q$, where ΔQ_s is the constant peak broadening in reciprocal space due to the finite-size effect, and the in-plane mosaic spread M, which does not depend on the momentum transfer Q. These three angular widths are related by

$$\omega^2(Q) = \omega_S^2(Q) + M^2 = \frac{\Delta Q_s^2}{Q^2} + M^2.$$

Hence, for each thickness, plotting of $\omega^2(Q)$ as a function of $1/Q^2$ allows deducing the mosaic spread M [Fig. 3(b)] and the domain size D [Fig. 3(c)]. The finite-size broadening is found to dominate over the mosaic spread up to $\theta \sim 10$, 7, and 5 ML for the Pd (200), (220), and (400) reflections, respectively. For large thickness, the widths of all Pd Bragg peaks arise primarily from the finite in-plane mosaic spread.

The in-plane mosaic spread [Fig. 3(b)] increases linearly with the logarithm of θ up to 18 ML where it reaches a maximum of 1.85°, and next decreases continuously, down to 0.6° for $\theta = 183$ ML.

The average in-plane domain size [Fig. 3(c)] increases continuously from 27 Å at $\theta = 0.58$ ML, up to 330 Å at $\theta = 183$ ML. Before the film gets continuous, this parameter is likely to be the average in-plane island size. Note that the values of $D = 29$ Å at 1 ML and $D = 34$ Å at 1.5 ML are very similar to one of the rare value (32 Å for $\theta = 1.2$ ML) obtained by scanning tunneling microscopy[42] (STM) for room-temperature growth of Pd on thin MgO(001) film. While the increase of the domain size is slow below 18 ML, there is a jump between 18 and 35 ML, as expected, because of channeling between islands.

The widths ΔQ_r of the Pd peaks measured in radial scans also have two contributions: ΔQ_s, due to the finite size of Pd crystallites, and $\Delta a/a \times Q$, due to the inhomogeneity $\Delta a/a$ of lattice parameters within the Pd. This inhomogeneous lattice parameter distribution can arise either from a strain within each island, or from different average lattice parameters between different islands. These radial widths are related by:

$$\Delta Q_r^2 = \Delta Q_S^2 + \left(\frac{\Delta a}{a}\right)^2 \times Q^2.$$

Hence, plotting $\ddot{A}Q_r^2$ as a function of Q^2 for different orders of reflections allows deducing again the domain size D, as well as the gradient $\Delta a/a$. The values obtained for D

are very close to those deduced from rocking scans but have larger error bars and are more scattered. The evolution of $\Delta a/a$ is reported in Fig. 3(d). The logarithm of $\Delta a/a$ is found to decrease linearly with the logarithm of θ. $\Delta a/a$ decreases from 0.13 at $\theta = 0.58$ ML, down to 0.007 for $\theta = 50$ ML, and is completely negligible for $\theta = 183$ ML. A comparison between $\Delta a/a \times Q$ and ΔQ_s shows that, along radial scans of all Pd Bragg peaks, for θ between 3 and 35 ML, the lattice parameter gradient effect dominates over the finite-size broadening. For the (200) reflection however, these two widths are very close to each other for all deposits.

During growth, wide radial scans around the (220) Bragg peaks were also performed at different l values to detect possible rods of scattering arising from stacking faults along the (111) plane.[43] In addition, wide radial scans were performed where diffraction peaks from twinned Pd should be detected if present.[44,45] In agreement with previous HRTEM measurements,[19] neither stacking faults nor twinning were found, whatever the amount of Pd deposited. 360°-wide rocking scans were also performed on the (200) and (220) Pd peaks, to look for other possible epitaxial relationships of Pd, such as (111)Pd‖(001)MgO, suggested by several other investigators,[32,33] and found in other systems, e.g., Pt/MgO(001).[46] No other epitaxial relationship than cube on cube was found.

All the above results show that measurements in radial and rocking scans of several orders of reflections are mandatory to get a complete description of the film crystalline quality and its evolution during growth.

B. Strain relaxation in Pd

From the preceding section, it appears that the major part of Pd has a lattice parameter close to that of bulk Pd. The analysis of the residual deformations in Pd may help to understand how this ''relaxed'' Pd is connected to the substrate.

We have seen that the shape of radial scans arises primarily from the distribution of lattice parameters in Pd, which is the result of an average over the strain distribution inside each island, and of an additional average over the different islands.

The scans along both the (h h 0) and (h 0 0) directions show that, below ~5 ML, Pd is partially strained, and the scattering by Pd is composed of only one peak. The islands are thus coherent with the substrate, i.e., with N MgO planes ''connected'' to N Pd planes. Above $\theta \sim 5$ ML, a shoulder appears at an h value of ~2.08, intermediate between that of MgO ($h = 2$) and that of Pd ($h = 2.1645$), revealing inhomogeneous deformations in Pd. We have already observed a similar behavior in the Ag/MgO(001) system.[44] Simulations were performed, which showed that this peak splitting arises from dislocations entering the island edges.

For the thickest film, when probing the whole thickness (at $\alpha = 0.3°$), and thus reaching the interface, a satellite is visible between the MgO and Pd peaks around $h = 2.08$ along the (h h 0.15) direction (Fig. 4) but no satellite is found along the (h 0 0.15) direction. We have demonstrated elsewhere in the case of Ag on MgO(001) (Refs. 45 and 47) that these satellites, which are also present on radial scans of higher order reflections, arise from an interfacial network of misfit edge dislocations, oriented along ⟨110⟩ directions, with $\frac{1}{2}[110]$ Burger's vectors. The spacing between dislocations (36 Å) corresponds to that of the O-lattice of the coincidence site lattice (CSL) model.[48] A network of misfit dislocations with the same orientation was previously observed by high-resolution transmission electron microscopy (HRTEM),[18,49,50] but for interfaces obtained by internal oxidation. We thus propose that the misfit edge dislocations that appear during growth at the edges of the islands reorder to form a regular network when the film gets continuous. This explains why, for $\alpha > \alpha_c^{Pd}$, along the (h 0 0.15) direction, the shoulder in between the MgO and Pd peaks progressively disappears above 18 ML, and has completely vanished above 35 ML (this evolution is not shown for $\alpha > \alpha_c^{Pd}$, but the result is clear for thick films, see Fig. 4).

C. Out-of plane measurements

An interesting observation is the pronounced decrease with increasing θ of the MgO CTR intensity at the (2 2 0.15) and (2 0 0.15) locations (Fig. 1). This decrease starts at the very beginning, even for $\theta = 0.2$ ML. If, above 18 ML, it can be attributed to the exponential damping of the transmitted beam in Pd, this is not the case below, and can only be explained by a strong destructive interference on the MgO CTR's. This section is devoted to the analysis of this effect, which allows determining the epitaxial site and interfacial distance.

The sharp truncation of the substrate is known to produce CTR's (Refs. 38 and 39) extending perpendicular to the surface, and connecting bulk Bragg peaks. Between Bragg peaks, the intensity variation is very sensitive to the structure of the interface. On the MgO(001) surface, two kinds of nonequivalent CTR's are present: ''strong''ones (whose intensity is proportional to the square of the sum of the atomic form factors of O and Mg), with h and k even, and ''weak'' ones (whose intensity is proportional to the square of the difference of the form factors), with h and k odd. They yield complementary information on the adsorption site.[30]

We have quantitatively measured the (20l), (31l) and (31l) MgO CTR's on the bare substrate and during the first stages of Pd deposition, between 0.2 and 12.5 ML. The CTR's were found to be everywhere resolution limited except around $l \sim 0$. The FWHM of the rocking curve of the anti-Bragg (110) CTR, which is not resolution limited, was found ~0.01°, which corresponds to an average terrace size of 6000 Å. For the bare substrate and for $\theta = 1$ and 2 ML, the CTR's were measured by rocking the sample around its surface normal for each l value. These rocking scans were background subtracted, integrated, normalized to constant monitor counts and corrected for polarization and Lorentz factors.[43,51,52] Most other measurements were performed directly in ''l scans'', i.e., along the CTR's, and corrected with a different Lorentz factor.[52] This is possible only because the intrinsic width of the MgO CTR's is everywhere (except close to $l = 0$) much smaller than the width induced by the experimental resolution, and because this width is not modified by the deposition of Pd, at least for $\theta < 12.5$ ML.

This last observation shows that the fraction of the Pd films that scatters at this location has the same correlation length as the substrate: the corresponding Pd atoms must be correlated via the substrate.

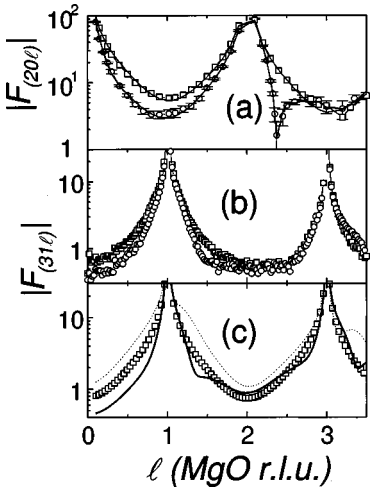

FIG. 5. Modulus of the structure factor of the (20l) and (31l) CTR's for the bare substrate and for 1 ML of Pd deposited. (a) (20l) CTR, obtained by integration and correction of rocking scans measurements, for the bare MgO(001) substrate (open squares with the line showing the best fit); and for $\theta=1$ ML of Pd deposited (open circles with error bars; the continuous line is the best fit). The best fits yielded the following parameter values: $d_{\text{Pd-MgO}}=2.22\pm0.02$ Å, $o_{\text{on-site}}=0.5\pm0.1$ ML, $\sigma_{\text{Pd}}=2.7\pm0.3$ Å, and $d_{\text{Pd-Pd}}=1.86\pm0.03$ Å (b) l-scan measurements of the (31l) CTR for the bare substrate (open squares) and after deposition of $\theta=1$ ML (open circles). (c) Calculated (31l) CTR, for the bare substrate (open squares), and for 1 ML of Pd deposited, with Pd above either Mg ions (dashed line) or O ions (thick continuous line).

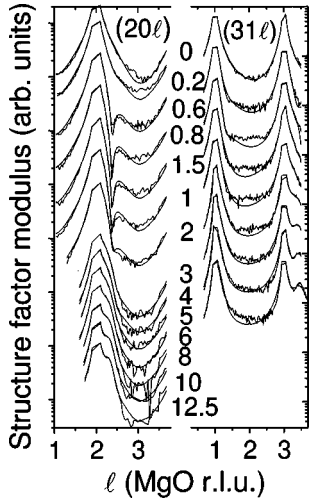

FIG. 6. Comparison between the measured (rough line) and calculated (smooth line) (20l) and (31l) CTR's during the room temperature growth of Pd on MgO(001). The modulus of the structure factor is reported as a function of the out-of-plane momentum transfer. Both CTR's have been simultaneously fitted over a large range of out-of-plane momentum transfer. The amount θ (in ML) of Pd deposited is indicated in the figure. The curves were vertically shifted for clarity.

Figure 5 shows the (20l) and (31l) CTR's for the bare substrate and for $\theta=1$ ML. Pd deposition drastically modifies the shape of the CTR's. On the (20l) CTR, it induces a pronounced decrease in the intensity between $l=0$ and 2, together with a sharp minimum around $l=2.35$. Along the (31l) CTR, a destructive interference is present both on the low-l and high-l sides of the (311) Bragg peak, and a positive interference on the right of the (333) peak. These modifications arise from the interference between the waves scattered by the substrate, and those scattered along the CTR by that fraction of the Pd film made of the Pd atoms correlated via the substrate. For simplicity, we will call these atoms ''registered'' or ''on site''. They are Pd atoms that sit on a lattice having the same in plane lattice parameter as the substrate. By fitting the experimental MgO CTR's with an appropriate model, it is possible to determine the position of the adsorption sites of ''on-site'' Pd atoms and several structural parameters of the ''on-site'' fraction.

The (20l) and (31l) CTR's were simultaneously fitted using a least-squares fitting procedure. The occupancy $o_{\text{on-site}}(z)$ of the ''on-site'' Pd plane located at a distance z above the last MgO plane was described by a complementary error function

$$o_{\text{on-site}}(z)=o_{\text{on-site}}\frac{1}{2N}\operatorname{erfc}\left(\frac{z}{\sqrt{2}\sigma_{\text{Pd}}}\right),$$

$$\text{where}\quad N=\sum_{\substack{\text{Ag}\\ \text{plane}\\ \text{nbi}}}\frac{1}{2}\operatorname{erfc}\left(\frac{z_i}{\sqrt{2}\sigma_{\text{Pd}}}\right).$$

The fitting parameters are the total amount of ''on-site'' Pd ($o_{\text{on-site}}$, in ML), the additional roughness σ_{Pd} of the ''on-site'' Pd with respect to the MgO substrate, the interfacial distance $d_{\text{Pd-MgO}}$, and the mean interplane (002) distance in the Pd film, $d_{\text{Pd-Pd}}$, that was supposed to be independent of the height with respect to the interface. The roughness is the root-mean squares averaging of the actual mean height of the ''on-site'' fraction and the variation of this height. The scale and the substrate roughness (2.4 Å rms) were first determined by a fit of the clean substrate CTR's (Fig. 5), the substrate roughness being modeled by a Gaussian distribution of terrace heights.[53] The MgO(001) substrate was assumed to be unaffected by the Pd deposit.

The best fits of the (20l) CTR for $\theta=0$ and 1 ML are reported in Fig. 5. Qualitatively, the sign of the interference along this CTR (with h and k even) allows discriminating between epitaxy on top of either oxygen or magnesium on the one hand, or above the octahedral site on the other hand. The strong destructive interference on the right-hand side of the (222) Bragg peaks allows excluding the possibility of the octahedral site. The parameters were $d_{\text{Pd-MgO}}=2.22\pm0.02$Å, $o_{\text{on-site}}=0.5\pm0.1$ ML, $\sigma_{\text{Pd}}=2.7\pm0.3$ Å, and $d_{\text{Pd-Pd}}=1.86\pm0.03$ Å. The measurement of a CTR with h and k odd is necessary to distinguish between the two remaining possible epitaxial sites: oxygen or magnesium. Fig. 5(c) shows the simulated (31l) CTR, using these parameters, for a Mg site, and for an O site. Clearly, *the epitaxial site is above oxygen atoms* of the substrate, and not Mg ones.

Then, for all deposits between $\theta=0$ and 12.5 ML, the (20l) and (31l) CTR's measured in l scans were simultaneously fitted over the ranges $l=1$ to 3.7 and 0.5 to 3.7, respectively, assuming the oxygen site. The best fits of the experimental data are reported in Fig. 6, and the corresponding parameters in Fig. 7. For all deposits, the agreement is good, which shows that the chosen model is adequate.

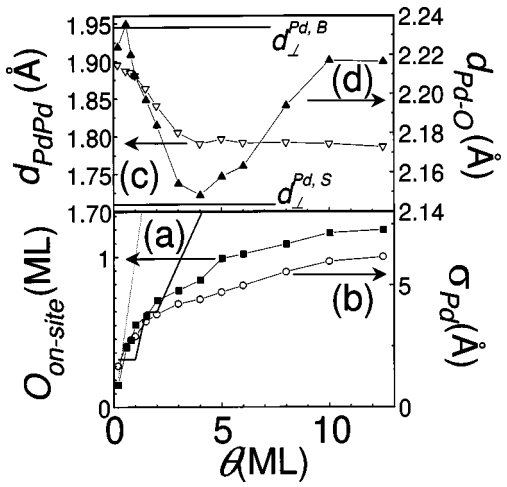

FIG. 7. (a). Evolution with the amount θ of deposited Pd of the four parameters used for fitting the CTR's (a) the total amount of ''on-site'' Pd expressed in number of ML (uncertainty estimated to ± 0.1 ML); lower curve, solid squares, left scale); the dashed line is the equivalent amount deposited θ; (b) the rms roughness of the ''on-site'' Pd (uncertainty estimated to ± 0.3 Å; lower curve, open circles, right scale); the continuous line is the equivalent height of the Pd deposited. (c) the (002) interplane distance in Pd d_{PdPd} (uncertainty estimated to ± 0.03 Å; upper curve, open triangles, left scale), horizontal lines indicate the bulk interplane distance $d_{\perp}^{\mathrm{Pd/B}}$, and the fully strained interplane distance $d_{\perp}^{\mathrm{PdS}}$ calculated in the framework of the linear elasticity theory; and (d) the interfacial distance $d_{\mathrm{Pd\text{-}O}}$ (uncertainty estimated to ± 0.02 Å; upper curve, solid triangles, right scale).

$o_{\mathrm{on\text{-}site}}$ [Fig. 7(a)] and σ_{Pd} [Fig. 7(b)] are found to first increase quickly with θ, and then slowly reach asymptotes around $\sim$1.3 ML and 6 Å respectively. $d_{\mathrm{Pd\text{-}Pd}}$ [Fig. 7(c)] decreases from 1.895 Å for $\theta = 0.2$ ML down to 1.79 Å for $\theta = 4$ ML, and next stays nearly constant, with only a very slight decrease down to 1.785 Å for $\theta = 12.5$ ML. Finally, $d_{\mathrm{Pd\text{-}O}}$ [Fig. 7(d)] shows a peculiar behavior: it first decreases from $\sim 2.23 \pm 0.03$ Å at $\theta = 0.5$ ML down to 2.15 ± 0.03 Å for $\theta = 4$ ML, and then increases to reach a steady state value of 2.22 ± 0.03 Å above 10 ML. Note that all these $d_{\mathrm{Pd\text{-}O}}$ values are very close to each other.

IV. DISCUSSION

In the following, the different results are discussed, and a model (schematically shown in Fig. 8) of the evolution of the structure and morphology during the room-temperature growth of Pd on an automatically flat and clean MgO(001) surface is proposed. These results are finally compared with those we previously obtained in the Ag/MgO(001) (Ref. 59) and Ni/MgO(001) (Ref. 31) systems, and similarities and differences are discussed on the basis of the different lattice parameter misfit and strength of the interfacial bonding.

A. Epitaxial site and interfacial distance

The above analysis unambiguously shows that the Pd atoms of the first monolayer sit on top of oxygen ions of the substrate. This contradicts previous conclusions drawn from SEELFS measurements,[16] that Pd would be on top of Mg ions. The present result is however in agreement with all recent theoretical predictions.[8,9,12,13] In particular, an *ab initio* full-potential linear muffin-tin orbital study of the electronic structure of a 1-ML Pd deposit on the MgO(001) surface[8] found a much smaller interfacial energy (-0.65 eV/atom) for Pd on top of O, as compared to Pd on top of Mg (-0.36 eV/atom). This result is also consistent with recent theoretical and experimental investigations of the epitaxial site of different metals on the MgO(001) surface, where the metal is Fe,[54] Ni,[9] Ag,[6] or Cu,[55,9] which all concluded to adsorption above oxygen. In addition, we have recently experimentally demonstrated that adsorption of Ag (Ref. 59 and Ni (Ref. 31) takes place above oxygen. We, thus, believe that the controversy concerning possible epitaxial sites is close to being over: in all cases, the epitaxial site is unique, atop the oxygen ions.

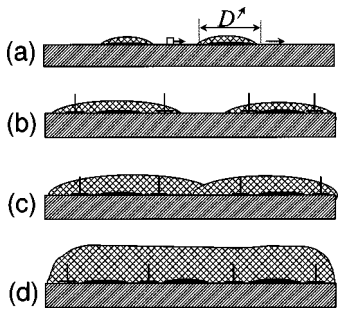

FIG. 8. Schematic representation of the evolution of the morphology and structure during the first stages of growth of Pd on MgO(001) at room temperature, as a function of the amount of Pd deposited θ. (a) Below 4–5 ML, coherent islands; (b) between 4–5 and 18 ML, incoherent islands with disordered dislocations; (c) between 18 and 35 ML, channeling between islands; (d) above 35 ML, continuous film with ordered dislocations. The Pd that is lattice-matched to the MgO parallel to the interface (i.e., pseudomorphic) is represented in black.

Whatever the deposit, the interfacial distance lies between 2.15 and 2.23 Å, with a steady-state value of 2.22 ± 0.03 Å. This is very close to the values of 2.18 Å for $\theta = 1$ ML and 2.225 Å for $\theta = 2$ ML calculated recently,[8,56] as well as to the theoretical value of 2.15 Å obtained for a single Pd atom adsorbed on top of the oxygen ions.[9,13]

This comparison, along with the epitaxial site, shows that, in the present Pd/MgO(001) case as well as in the case of the Ag/MgO(001) (Ref. 59) and and Ni/MgO(001) (Ref. 31) interfaces, the latest theoretical models are fairly accurate to calculate the main structural characteristics of these relatively simple interfaces.

B. Pseudomorphic Pd

The evolution with θ of the structural parameters describing the ''on-site'' fraction contains a lot of information, in particular on the nature of this ''on-site'' fraction.

Let us first look at the roughness. As shown in Fig. 7(b), below $\theta = 2$ ML, the roughness of the ''on-site'' fraction (i.e., its average height) is equal to the equivalent height of Pd deposited. It next remains much smaller than this equivalent height, reaching only the height of 3 atomic planes for $\theta = 12.5$ ML. This shows that the ''on-site'' fraction is confined near the interface between Pd and MgO(001). In addition, at the very beginning ($\theta < 0.5$ ML), the ''on-site'' oc-

cupancy [Fig. 7(a)] is nearly equal to the amount deposited: the fraction of Pd that is already relaxed is much smaller than the pseudomorphic fraction. For $\theta = 1$ ML, $O_{\text{on-site}} \sim 0.5$: half of the amount deposited is ''on site'' and located at the interface. The ''on-site'' occupancy next increases only much more slowly than θ, saturating around $O_{\text{on-site}} = 1.2$ ML for large deposited amounts. From these observations, we conclude that, for all deposited amounts, most of the ''on-site'' Pd is composed of a pseudomorphic Pd layer, i.e., a Pd layer that is lattice matched with MgO parallel to the surface, and is located either at the interface or in the next two Pd layers. This is confirmed by the fact that the same scale factor is obtained when fitting CTR's of different orders, which would not be the case[59] if the interferences along the CTR's were arising from relaxed Pd. This pseudomorphic Pd is schematically represented in black in Fig. 8, at the interface, below the relaxed Pd islands (note that, in the middle of each island, for symmetry reason, there should be a column of Pd atoms that are also perfectly ''on site'', although not pseudomorphic; this column also participates weakly to the parameters of the ''on-site'' fraction deduced from the measurements; hence, in particular, the thickness of the pseudomorphic part is very slightly overestimated). Our conclusions are in agreement with previous HRTEM (Refs. 20 and 18) as well as SEELFS (Refs. 19 and 28) measurements, which show that the first Pd layer at the interface is laterally expanded to adopt the lattice parameter of MgO.

The out-of plane Pd-Pd distance may be compared to the (002) bulk Pd interplanar distance, $d_{\perp}^{\text{Pd,R}} = 1.945$ Å, and to the value of $d_{\perp}^{\text{Pd,S}} = 1.71$ Å calculated in the framework of linear elasticity for Pd strained in plane to the MgO(001) substrate. This latter is deduced from the lattice parameters according to: $d_{\perp}^{\text{Pd,S}} - d_{\perp}^{\text{Pd,R}} / d_{\perp}^{\text{Pd,B}} = -2 \times C_{12}/C_{11} \times a_{\parallel}^{\text{Pd,S}} - a_{\parallel}^{\text{Pd,B}} / a_{\parallel}^{\text{Pd,S}}$ where C_{11} and C_{12} are the elastic constants of Pd (2.271×10^{11} Pa and 1.761×10^{11} Pa, respectively), $a_{\parallel}^{\text{Pd,S}}$ is the in-plane lattice parameter of Pd strained by the MgO substrate (i.e., the MgO lattice parameter), and $a_{\parallel}^{\text{Pd,B}}$ is the bulk Pd lattice parameter. For all deposits, the interplane distance is intermediate between these two values. At the beginning of deposition, it is closer to the bulk value, and decreases down to a nearly constant value closer to that of elastically strained Pd for $\theta > 4$ ML. At the beginning, the ''on-site'' Pd has a thickness limited to one or two atomic layers, so that the elasticity theory cannot be applied. Since it is covered and surrounded by relaxed Pd (see Fig. 8), a value close to the bulk one is not surprising. As the thickness increases, below $\theta = 4-5$ ML, the elasticity theory becomes a better approximation. However, the islands are now composed mainly of relaxed Pd and a small amount of pseudomorphic Pd. This explains the decrease of the interplane distance, while still being larger than $d_{\perp}^{\text{Pd,S}}$.

The fact that both the interfacial distance and the Pd interplane distance show a discontinuity around $\theta = 4-5$ ML can be correlated to the onset of plastic relaxation for this amount of Pd deposited. Above 4–5 ML, dislocations are introduced at the island edges relaxing the misfit, and the ''on-site'' fraction becomes confined in the regions of ''good match'' between the Pd and MgO lattices, i.e., laterally located between two misfit dislocations lines. At these locations, the ''on-site'' Pd is close to truly pseudomorphic, which explains the value of the Pd interplane distance. However, the out-of-plane interplanar distance should no longer be compared to elastic calculation of strained Pd, but rather to a full calculation of the atomic positions between two misfit dislocations, which is beyond the scope of the present study.

Above $\theta = 4-5$ ML, the increase of the interfacial distance would correspond to a weakening of the metal/oxide bond as the interfacial atoms become less isolated, i.e., as they are more and more involved in the metallic bounding of the Pd film. An increase of the interfacial distance with θ is actually what is predicted by *ab initio* calculations[56,57] and is the tendency that is intuitively expected. Why the interfacial distance decreases at the very beginning of deposition is less clear. A tentative explanation would be correlated with a decreasing aspect ratio (height over lateral extension) of the islands with increasing θ. As this aspect ratio would decrease, the influence of ''metallic'' bonding versus interfacial bonding would also decrease, resulting in a shorter interfacial distance.

C. Structure and morphology during growth

Recent HRTEM observations of the growth morphology at room temperature,[26] revealed that the islands are rather ragged, with no well-defined surface plane, which is fully consistent with the evolution of α_c below 18 MI. The Pd in these small islands is coherent with MgO and a large strain induced by the substrate is present, which decreases with increasing island size. We propose that the relaxation is done near the edges of the islands because the surfaces are free to deform, which is in agreement with recent HRTEM results.[18,20,58]

Above $\theta = 4-5$ ML, the Pd becomes incoherent, with introduction of misfit dislocations at the edges of the islands. We have seen that, below 4–5 ML, the islands grow in size while being strained by the substrate, with the first atomic layer at the interface being nearly pseudomorphic. Hence, large strains are accumulated in this pseudomorphic layer, and also in the partially relaxed Pd located near the edges of the islands (see Fig. 8). The corresponding elastic energy stored in the Pd film increases with the island size. We propose that, around 4–5 ML, the island size reaches a critical size above which it becomes energetically more favorable to release part of this strain by introducing dislocations near the edges, where the elastic energy stored is maximal. This picture is consistent with the rapid decrease [Fig. 3(a)] of the average in-plane lattice parameter up to $\theta = 5$ ML, followed by the much slower decrease after the lattice parameter misfit has been relaxed by the introduction of misfit dislocations.

The increase of the mosaic spread up to ~30 ML shows that small finite rotations of the islands is probably an additional relaxation process helping to minimize the strain energy stored in the pseudomorphic or partially strained Pd.[40] As the islands grow in size, thus storing more and more elastic energy at the interface, they undergo larger and larger rotations up to a point, above 18 ML, where connections between islands start to form, resulting in a reorientation of the islands with respect to each other, and in the average, to a decrease of the mosaic spread.[40] In addition, new defects such as grain boundaries or misfit dislocations are likely to

be introduced when islands coalesce into very wide islands, which again help relaxing the elastic energy. This results in a continuous decrease of the mosaic spread above $\theta = 18$ ML.

The onset of reordering of interfacial dislocations is presumably responsible for the increase of the domain size measured on the top of the Pd islands.

The continuous decrease of $\Delta a/a$ and the increase of the domain size reveal the decreasing influence of the substrate on the film as this later grows thicker. After the film is continuous, the domain size becomes large because very few new defects have to be introduced during growth.

Before going on, our results should be compared to a previous combined GIXS and TEM study of the growth of Pd on MgO(001).[32,33] The main differences with the present study are the higher deposition rate (1 Å/s instead of 1 Å/min), the higher substrate temperatures (100, 300, and 600 °C), the substrate preparation conditions (polished and then *in situ* annealed), and the higher pressure (3×10^{-7} Torr) during deposition. In addition, the GIXS experiments were performed *ex situ* with a laboratory source, on different samples with different thickness. Consequently, the resolution in momentum was poor, and only films thicker than 10 Å could be investigated. Most of the Pd was found in cube-on-cube epitaxy, but the peculiar shape reported here of the Pd scattering was not observed, neither the satellite arising from interfacial dislocations. Other orientational relationships were reported, which are not found in the present study. These may have been induced either by surface defect, or by surface contamination. The CTR's were not measured, so no information was deduced on the epitaxial site and interfacial distance.

D. Comparison with the Ag/MgO(001) and Ni/MgO(001) interfaces

In order to better understand the basic physical phenomena governing the interfacial structure, i.e., the parameters of the interface and the residual deformations within the metal islands, it is interesting to compare similar systems with systematic variations of some physically relevant parameters, among which the lattice parameter misfit and the strength of the interfacial bonding. Indeed, the final state of the islands results from a competition between different mechanisms. The larger the lattice parameter misfit, the sooner the introduction of misfit dislocation or other misfit releasing defects is expected. Also, intuitively, the larger the misfit and the larger the metal stiffness, the less likely the metal is to be strained by the substrate. At the opposite, the stronger the interfacial bonding, the stronger the tendency of the metal to be strained by the substrate, and possibly to form a fully lattice-matched (pseudomorphic) interfacial layer.

We have systematically investigated by GIXS the structure and morphology of three metal/MgO(001) interfaces during their *in situ* growth at room temperature for three different metals, Ag,[59] Pd, and Ni.[31] In all three cases, the metal has a fcc structure and the epitaxy is cube on cube. The misfit at these three interfaces shows a systematic trend, increasing from 2.98% for Ag, to 7.64% for Pd, and −6.4% for Ni. According to many recent theoretical calculations, the strength of the metal-oxide bond also varies significantly, in the same order. For Ag, the binding is weak, of physisorption type, between 0.1 and 0.3 eV/atom,[2,6,27,57,60–67] and mostly of electrostatic origin, while for Pd and Ni, the bond is mostly polar covalent and ranges from 0.65[8] to 0.81[67] eV/atom for Pd, and from 0.88[67] to 1.24[9] eV/atom for Ni. Comparison of the elastic constants of the three metals also shows that Ag is much softer than Pd and Ni. On the other hand differences between the crystal-vapor surface energies of the three metals can be neglected in a first approximation.[68] Apart from the common three-dimensional growth mode, which is expected by simple thermodynamic arguments, these three interfaces indeed exhibit fairly different characteristics. For Ag and Pd thick films, the lattice parameter misfit is simply relaxed by a network of interfacial misfit dislocations, while for Ni, the relaxation is performed by the growth, in addition to cube-on-cube Ni, of Ni clusters in Ni(110)‖MgO(001) epitaxy, with four different in-plane orientational relationships.[31] The absence of ordered misfit dislocations at the Ni/MgO(001) interface is not surprising because the large value of the misfit implies alternative relaxation processes.

More interesting is the state of strain in the metal clusters as a function of their size (or of the deposited amount). At the very beginning of the growth, the islands are very small (with a size smaller than 100 Å), and thus have a large surface over volume ratio. It is well known that, if such small clusters would be free standing, the average lattice parameter would be much smaller than the bulk parameter. For instance, a numerical simulation[69] yields 3% and 1.4% smaller lattice parameters for hemiellipsoidal Ag islands of 100 and 700 atoms, respectively. As shown for very small clusters in the case of Ni and Cu,[9,55] when these clusters are absorbed onto MgO, which has a larger lattice parameter, the average interatomic distance tends to be intermediate between that of the free cluster and that of MgO because of the interfacial potential. The larger the interfacial bonding, the larger the metal average interatomic spacing.

The in-plane diffraction data show that, at the very beginning of the growth ($\theta \sim 0.5$ ML), the average lattice parameter is very close to that of the bulk for Ag, nearly in between that of the bulk and that of MgO for Pd, and only slightly larger than the bulk one for Ni. While the trend for Ni could be anticipated because of the very large misfit, the comparison between Ag and Pd is somewhat contrary to intuition since Ag is softer and has a smaller misfit, so that the elastic energy due to residual deformations is expected to be smaller for strained Ag than for strained Pd. This effect actually reveals the much weaker binding of Ag with MgO, as compared to Pd. The Ag-MgO bond is so weak that the free-surface effect fully dominates for small clusters.[59] By comparison, although Pd is stronger and displays a larger misfit with MgO, its binding to MgO is strong enough to partially overcome both the residual deformation elastic energy and the free-surface effect.

The difference between the three metals is even clearer when comparing the parameters of the ''on-site'' fraction. The significant decrease of the interfacial distance, from 2.52 Å for Ag to 2.22 Å for Pd and 1.88 Å for Ni, directly reflects the increasing strength of the interfacial bond. The most striking differences however lie in the amount and height of the ''on-site'' fraction, at the beginning of the growth, between $\theta = 0$ and 10 ML. For Pd and Ni, the amount of ''on-

site'' metal saturates around 1.2 ML for large θ, and its average height saturates around 2 to 3 atomic planes. This shows that, in both cases, a significant fraction of the interfacial atoms is fully lattice-matched laterally with the MgO substrate. The larger misfit for Ni is compensated by its stronger bonding with MgO, yielding a very similar pseudomorphic fraction in both cases. Very different is the case of Ag, with an extremely small amount of ''on-site'' Ag (less than 0.1 ML for $\theta = 0.5$ ML) extending over a very large height, reaching 15 atomic planes for $\theta = 10$ ML. This, together with the other scattering measurements, could only be interpreted by the absence of lattice-matched Ag at the interface.[59] Despite the small lattice parameter misfit and the softness of Ag, which implies a lesser cost of residual deformations as compared to Pd and Ni, all the Ag within the islands has a lattice parameter close to that of bulk Ag even at the interface. This effect can only be explained by the very weak binding at the Ag-MgO interface. The larger island aspect ratio ($\sim$0.4) in the case of Ag as compared to Pd or Ni ($\sim$0.2) is another indication of this difference in interfacial bond strength.

From all the above comparisons, we may conclude that the structure and morphology at these metal/MgO interfaces are mostly influenced by the strength of the bonding at the interface, rather than by the lattice parameter misfit.

On the other hand, the presence or absence of twins and stacking faults seems to be connected to the bulk properties. A significant tendency to twinning and stacking faults was evidenced for Ag,[59] while neither twins nor stacking faults were found in the cases of Ni (Ref. 31) and Pd. This is in agreement with the much larger twin boundary and stacking fault energies in Ni [125 mJ/m^2 (Ref. 70) and 43 mJ/m^2 (Ref. 71), respectively] and Pd [180 mJ/m^2 for the twinning energy (Ref. 72)] as compared to Ag [16 mJ/m^2 (Ref. 73), respectively].

V. CONCLUSIONS

In summary, at room temperature, for a deposition rate of 0.5 ML/min, the growth of Pd on an atomically flat MgO(001) surface is confirmed to proceed by nucleation, growth and coalescence of islands from the very beginning of the deposition (0.2 ML). The Pd deposited is in cube-on-cube epitaxy. Neither stacking faults nor twins were found. Below 4–5 ML, most of the Pd is coherent with the MgO substrate. The monolayer closest to the interface is mostly pseudomorphic, while the remaining Pd has a lattice parameter close to the bulk one, thanks to relaxation at the edges and on the free surfaces of the islands. Around 4–5 ML, misfit dislocations are introduced at the edges of the islands. New dislocations probably continue to appear at the Pd islands edges as the islands grow laterally. Large flat islands appear near 18 ML, and the film becomes continuous around 35 ML. Above 35 ML, the dislocations that are buried at the interface reorganize into an ordered network.

A new, quantitative analysis of the MgO CTR's allowed for the first time the determination of the adsorption site and interfacial distance, as well as a description of the morphology of the deposit for very small Pd amounts. The epitaxial site is unambiguously shown to be Pd above O ions of the last MgO(001) plane, and the steady-state value of the interfacial distance is found to be $d_{\text{Pd-MgO}} = 2.22 \pm 0.03$ Å. These two results are consistent with the most recent theoretical calculations.

Comparison with similar measurements for the Ag/MgO and Ni/MgO(001) interfaces shows that the main differences between the interfacial characteristics in the three systems mostly arise from the largely differing strength of the metal-oxide bond, rather than the lattice parameter misfit.

ACKNOWLEDGMENTS

We would like to thank A. Stierle and the staff of the ID32 beamline for help during the measurements.

*Author to whom correspondence should be addressed. FAX:(33) 4 76 88 51 38. Electronic address: grenaud@cea.fr

†Laboratory associated with the Joseph Fourier University, Grenoble, France.

[1] See, e.g., C. T. Campbell, Surf. Sci. Rep. **27**, 1 (1997); R. J. Lad, Surf. Rev. Lett. **2**, 109 (1995).

[2] M. W. Finnis, A. M. Stoneham, and P. W. Tasker, *Metal-Ceramic Interfaces*, Acta Scripta Metall. Proceedings Series Vol. 4 (Pergamon, New York, 1990).

[3] V. E. Henrich and P. A. Cox, *The Surface Science of Metal Oxides* (Cambridge University Press, Cambridge, 1994).

[4] For different articles on the subject, see *Proceedings of the International Symposium on Metal-Ceramic Interfaces* [Acta Metall. Mater. Suppl. 40 (1992)].

[5] M. W. Finnis, J. Phys.: Condens. Matter **8**, 5811 (1996).

[6] J. R. Smith, T. Hong, and D. J. Srolovitz, Phys. Rev. Lett. **72**, 4021 (1994).

[7] C. Noguera, *Physics and Chemistry at Oxide Surfaces* (Cambridge University Press, Cambridge, 1996).

[8] J. Goniakowski, Phys. Rev. B **57**, 1935 (1998).

[9] G. Pacchioni and N. Rösch, J. Chem. Phys. **104**, 7329 (1996).

[10] P. Palmberg, T. Rhodin, and C. Todd, Appl. Phys. Lett. **11**, 33 (1967).

[11] O. Robach, G. Renaud, and A. Barbier, Surf. Sci. **401**, 227 (1998).

[12] A. M. Ferrari and G. Pacchioni, J. Phys. Chem. **100**, 9032 (1996).

[13] I. Yudanov, G. Pacchioni, K. Neyman, and N. Rösch, J. Phys. Chem. B **101**, 2786 (1997).

[14] K. Yamamoto, Y. Kasukabe, R. Takeishi, and T. Osaka, J. Vac. Sci. Technol. A **14**, 327 (1996).

[15] A. Stirling, I. Gunji, A. Endou, Y. Oumi, M. Kubo, and A. Miyatomo, J. Chem. Soc., Faraday Trans. **93**, 1175 (1997).

[16] C. Goyhenex and C. R. Henry, J. Electron Spectrosc. Relat. Phenom. **61**, 65 (1992).

[17] D. W. Goodman, Surf. Rev. Lett. **2**, 9 (1995).

[18] K. Heinemann, T. Osaka, H. Poppa, and M. Avalos-Borja, J. Catal. **83**, 61 (1983).

[19] C. Goyenex, C. R. Henry, and J. Urban, Philos. Mag. A **69**, 1073 (1994).

[20] S. Giorgo, C. Chapon, C. R. Henry, and G. Nihoul, Philos. Mag. B **67**, 773 (1993).

[21] M. Meunier and C. R. Henry, Surf. Sci. **307-309**, 514 (1994).

[22] M. Meunier, Ph.D. thesis, University of Aix-Marseille, 1995.

[23] A. Renou and A. Rudra, Surf. Sci. **156**, 69 (1985).

[24] C. R. Henry, Surf. Sci. Rep. **31**, 231 (1998).

[25] C. R. Henry, C. Chapon, C. Duriez, and S. Giorgio, Surf. Sci. **253**, 177 (1991).
[26] C. R. Henry and M. Meunier, Mater. Sci. Eng., A **217/218**, 239 (1996).
[27] T. Hong, J. R. Smith, and D. J. Srolovitz, Acta Metall. Mater. **43**, 2721 (1995).
[28] S. Bartuschat and J. Urban, Philos. Mag. A **76**, 783 (1997).
[29] I. K. Robinson and D. J. Tweet, Rep. Prog. Phys. **55**, 599 (1992).
[30] P. Guénard, G. Renaud, and B. Villette, Physica B **221**, 205 (1996).
[31] A. Barbier, G. Renaud, and O. Robach, J. Appl. Phys. **84**, 4259 (1998).
[32] H. Fornander, L. Hultman, J. Birch, and J.-E. Sundgren, J. Cryst. Growth **186**, 189 (1998).
[33] H. Fornander, J. Birch, L. Hultman, L.-J. Petersson, and J.-E. Sundgren, Appl. Phys. Lett. **68**, 2636 (1996).
[34] G. Renaud, B. Villette, and P. Guénard, Nucl. Instrum. Methods Phys. Res. B **95**, 422 (1995).
[35] ESRF beamline Handbook, http://www.esrf.fr
[36] K. W. Evans-Lutterodt and Mau-Tsu Tang, J. Appl. Crystallogr. **28**, 318 (1995).
[37] C. Goyhenex, M. Meunier, and C. R. Henry, Surf. Sci. **350**, 103 (1996).
[38] I. K. Robinson, Phys. Rev. B **33**, 3830 (1986).
[39] S. R. Andrews and R. A. Cowley, J. Phys. C **18**, 6247 (1985).
[40] D. W. Pashley, M. J. Stowell, M. H. Jacobs, and T. J. Law, Philos. Mag. **10**, 127 (1964); D. W. Pashley, Adv. Phys. **14**, 327 (1965).
[41] C. R. Henry, C. Chapon, S. Giorgio, and C. Goyhenex, *Chemisorption and Reactivity of Clusters and Thin Films*, Vol. 331 of *NATO Advanced Study Institute Series E: Applied Sciences*, edited by R. M. Lambert and G. Pacchioni (Kluwer, Dordrecht, 1997), p. 117.
[42] C. Xu, W. S. Oh, G. Liu, D. Y. Kim, and D. W. Goodman, J. Vac. Sci. Technol. A **15**, 1261 (1997).
[43] P. Guénard, Ph.D. thesis, University of Grenoble, 1996.
[44] O. Robach, G. Renaud, A. Barbier, and P. Guénard, Surf. Rev. Lett. **5**, 359 (1997).
[45] G. Renaud, P. Guénard, and A. Barbier, Phys. Rev. B **58**, 7310 (1998).
[46] P. C. McIntyre, C. J. Maggiore, and N. Nastasi, Acta Mater. **45**, 869 (1997); **45**, 879 (1997).
[47] P. Guénard, G. Renaud, B. Villette, M. H. Yang, and C. P. Flynn, Scr. Metall. Mater. **31**, 1221 (1994).
[48] W. Bollmann, *Crystal Defects and Crystalline Interfaces* (Springer, Berlin, 1970).
[49] P. Lu and F. Cosandey, Ultramicroscopy **40**, 271 (1992).
[50] P. Lu and F. Cosandey, Acta Metall. Mater. **40**, S259 (1992).
[51] E. Vlieg, J. Appl. Crystallogr. **30**, 532 (1997).
[52] O. Robach, Ph.D. thesis, University of Grenoble, 1997.
[53] J. Harada, Acta Crystallogr., Sect. A: Found. Crystallogr. **48**, 764 (1992).
[54] T. Urano and T. Kanaji, J. Phys. Soc. Jpn. **57**, 3403 (1988).
[55] V. Musolino, A. Selloni, and R. Car, J. Chem. Phys. **108**, 5044 (1998).
[56] J. Goniakowski, Phys. Rev. B **58**, 1189 (1998).
[57] L. Spiess, Surf. Rev. Lett. **3**, 1365 (1996).
[58] S. Giorgio, C. R. Henry, C. Chapon, and C. Roucea, J. Catal. **148**, 534 (1994).
[59] O. Robach, G. Renaud, and A. Barbier, Phys. Rev. B (to be published).
[60] J. Purton, S. C. Parker, and D. W. Bullet, J. Phys.: Condens. Matter **9**, 5709 (1997).
[61] P. Blöchl, G. P. Das, H. F. Fischmeister, and U. Schönberger, in *Metal-Ceramic Interfaces*, edited by M. Rühle, A. G. Evans, M. F. Ashby, and J. P. Hirth (Pergamon Press, Oxford, 1990), p. 9.
[62] E. Heifets, F. Y. Zhukovskii, E. A. Kotomin, and M. Causa, Chem. Phys. Lett. **283**, 395 (1998).
[63] E. Heifets, E. A. Kotomin, and R. Orlando, J. Phys.: Condens. Matter **8**, 6577 (1996).
[64] C. Li, R. Wu, A. J. Freeman, and C. L. Fu, Phys. Rev. B **48**, 8317 (1993).
[65] H. X. Liu, H. L. Zhang, H. L. Ren, S. X. Ouyang, and R. Z. Yuan, Ceram. Int. **22**, 79 (1996).
[66] U. Schönberger, O. K. Andersen, and M. Methfessel, Acta Metall. Mater. **40**, S1 (1992).
[67] N. Rösch and G. Pacchioni, in *Chemisorption and Reactivity on Supported Clusters and Thin Films*, Vol. 331 of *NATO Advanced Study Institute Series E: Applied Sciences*, edited by R. M. Lambert and G. Pacchioni (Kluwer, Dordrecht, 1997), p. 353.
[68] J. P. Hirth and J. Lothe, *Theory of Dislocations* (Krieger, Malabar, FL, 1992), Appendix 2, p. 838.
[69] F. Lançon and T. Deutsch (private communication).
[70] C. B. Carter and S. M. Holmes, Philos. Mag. **35**, 1161 (1977).
[71] L. E. Murr, *Interfacial Phenomena in Metals and Alloys* (Addison-Wesley, Reading, MA, 1975).
[72] I. L. Dillamore and R. E. Smallman, Philos. Mag. **12**, 191 (1965).
[73] H. Saka, T. Iwata, and T. Imura, Philos. Mag. A **37**, 273 (1978).